

Neutron scattering study of spin dynamics in superconducting (Tl,Rb)₂Fe₄Se₅Songxue Chi,¹ Feng Ye,^{1,2} Wei Bao,^{3,*} Minghu Fang,⁴ H. D. Wang,⁴ C. H. Dong,⁴ A. T. Savici,⁵ G. E. Granroth,¹ M. B. Stone,¹ and R. S. Fishman⁶¹Quantum Condensed Matter Division, Oak Ridge National Laboratory, Oak Ridge, Tennessee 37831, USA²Department of Physics and Astronomy, University of Kentucky, Lexington, Kentucky 40506, USA³Department of Physics, Renmin University of China, Beijing 100872, China⁴Department of Physics, Zhejiang University, Hangzhou 310027, China⁵Neutron Data Analysis and Visualization Division, Oak Ridge National Laboratory, Oak Ridge, Tennessee 37831, USA⁶Materials Science and Technology Division, Oak Ridge National Laboratory, Oak Ridge, Tennessee 37831, USA

(Received 11 January 2013; revised manuscript received 21 February 2013; published 4 March 2013)

We observed in superconducting (Tl,Rb)₂Fe₄Se₅ spin-wave branches that span an energy range from 6.5 to 209 meV. Spin dynamics are successfully described by a Heisenberg localized spin model whose dominant in-plane interactions include only the nearest (J_1 and J'_1) and next nearest neighbor (J_2 and J'_2) exchange terms within and between the tetramer spin blocks, respectively. These experimentally determined exchange constants would crucially constrain the theoretical viewpoints on magnetism and superconductivity in the Fe-based materials.

DOI: 10.1103/PhysRevB.87.100501

PACS number(s): 74.25.Ha, 74.25.Jb, 74.70.-b, 78.70.Nx

One astonishing aspect of the recently discovered $T_c \sim 30$ K iron selenide superconductors^{1–5} is the coexistence of a large magnetic moment ($3.3\mu_B/\text{Fe}$) and high transition-temperature ($T_N \approx 470\text{--}560$ K) antiferromagnetic order.^{6,7} Different from all other families of the Fe-based superconductors, the new iron selenide superconductors consist of Fe plates with highly ordered $\sqrt{5} \times \sqrt{5}$ vacancy superstructure.^{6–8} Samples with less developed $\sqrt{5} \times \sqrt{5}$ order are known to *not* be superconducting either when their compositions are close to⁹ or deviate significantly from¹⁰ the ideal $A_2\text{Fe}_4\text{Se}_5$ formulas. In the latter case, an additional phase of orthorhombic vacancy order with a $\sqrt{2} \times \sqrt{2}$ or $2\sqrt{2} \times \sqrt{2}$ unit cell also exists at intermediate temperatures. The large-moment block antiferromagnetic order developed on the vacancy ordered Fe lattice [Figs. 1(a)–1(b)] exists in superconducting as well as insulating samples.¹⁰

The perfect $\sqrt{5} \times \sqrt{5}$ vacancy order demands one vacancy per five Fe ions and the charge neutrality enforces a proportional number of intercalating A ions. While superconductivity can tolerate, or even requires, a small composition deviation from the ideal $A_2\text{Fe}_4\text{Se}_5$ to dope charges, the crystal structure has to deform, as expected in any nonstoichiometric samples, such that the “vacant” Fe1 site is found to be occupied by a few percent of Fe on average^{6,8} and fine-scale structural variation^{11,12} and phase separation¹³ are observed in superconducting samples. Nonetheless, the block antiferromagnetic order not only coexists with superconductivity in the same sample,^{6,7,12,14} but also the interaction between these two long-range ordered states reveals itself in an anomalous magnetic order parameter near T_c .^{6,7,15} Irrespective of the current theoretical debate on the role played by spin excitations in forming the superconducting Cooper pairs,^{16–18} it is important to investigate spin dynamics experimentally in the new iron selenide superconductors to bound the discussion.

Here we report inelastic neutron scattering measurements covering the whole spin excitation spectrum in the (Tl,Rb)₂Fe₄Se₅ superconductor. Four doubly degenerate spin-wave branches, one acoustic and three optical, form in three groups and span an energy range up to ~ 210 meV [Fig. 1(c)]. A

Heisenberg model, involving the intra- and interblock nearest and next nearest neighbor interactions in the Fe plane and the nearest neighbor interaction between the planes, is sufficient to describe our data. Consistent with *ab initio* theoretical works, there is no need to resort to the third nearest neighbor exchange interaction J_3 .

Single crystals of (Tl,Rb)₂Fe₄Se₅ ($T_c \approx 32$ K) were grown using the Bridgman method.⁵ A small single crystal was used in a neutron diffraction study to determine the crystalline and magnetic structural properties.⁷ For the inelastic studies, 240 platelike crystals were mutually aligned on Al plates using an x-ray Laue diffractometer. The final assembly has a net sample mass of 19.5 g. The sample was sealed with He exchange gas inside an Al can¹⁹ and measured with the SEQUOIA^{20,21} fine resolution and the ARCS²² wide angular range Fermi chopper spectrometers at the Spallation Neutron Source (SNS) at Oak Ridge National Laboratory (ORNL). Neutron beams of incident energy $E_i = 50, 100, 200,$ and 350 meV were provided by the coarser resolution Fermi chopper²¹ spinning at 180, 240, 360, and 420 Hz, respectively, on SEQUOIA. For ARCS $E_i = 400$ meV was provided by the 700 meV Fermi chopper spinning at 420 Hz. The sample was kept in its ground state by a closed cycle refrigerator operating at $T \approx 6$ K. We will label the wave vector transfer $\mathbf{Q} = (H, K, L)$ using the tetragonal $I4/m$ unit cell⁶ of $a = 8.683$ and $c = 14.39$ Å.

The importance of the nearest and next nearest neighbor exchange interactions in the Fe plane was identified in the initial *ab initio* study examining the iron pnictide superconductors.²³ The lattice tetramerization forms the spin quartet block [Fig. 1(b)] making the intra- and interblock exchange interactions inequivalent.²⁴ Therefore, the effective Heisenberg Hamiltonian

$$H = \sum_{i,j} J_{i,j} S_i \cdot S_j - \Delta \sum_i S_{iz}^2 \quad (1)$$

is used which includes five exchange constants $J_1, J_2, J'_1, J'_2,$ and J_c as depicted in Figs. 1(a) and 1(b), and the single-ion anisotropy constant Δ that quantifies the observed Fe spin $S = 3.2(1)/g$ alignment along the c axis.⁷ This spin model on

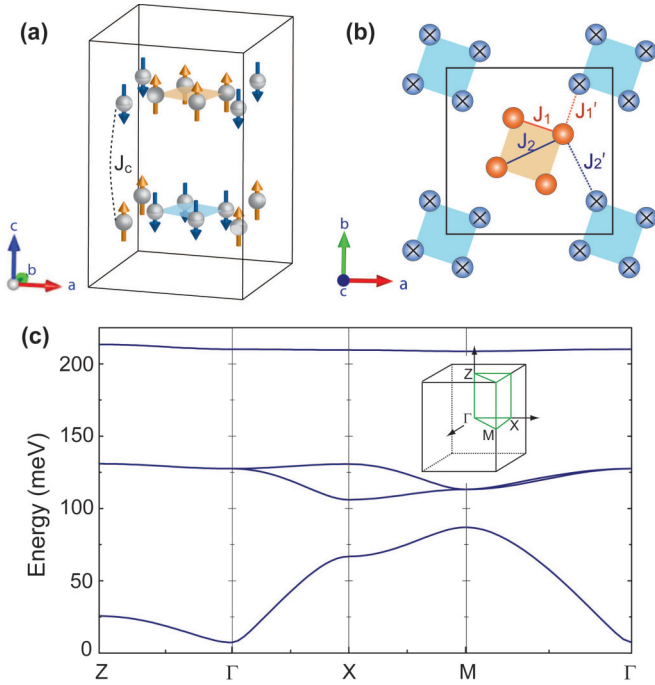


FIG. 1. (Color online) (a) Schematic diagram of the block antiferromagnetic structure in the $14/m$ unit cell. Only Fe ions with their spin directions are shown. J_c is the exchange interaction between spins in adjacent Fe planes. (b) Each shaded square highlights a block of four ferromagnetically coupled Fe^{2+} ions in the Fe plane. The open (orange) and the crossed (blue) balls represent spins with opposite directions perpendicular to the ab plane. The black line marks the unit cell. The four unique in-plane exchange interactions considered in this work are labeled. (c) Theoretical spin-wave dispersions calculated using experimentally determined parameters.

the $\sqrt{5} \times \sqrt{5}$ vacancy ordered lattice has been theoretically investigated^{25,26} and, as to be shown later, describes the spin dynamics of $(\text{Tl,Rb})_2\text{Fe}_4\text{Se}_5$.

Figure 2 shows the evolution of the acoustic branch of spin waves with increasing energy in $(\text{Tl,Rb})_2\text{Fe}_4\text{Se}_5$. The orientation of the tetramer Fe block with respect to the $14/m$ unit cell can be clockwise [Fig. 1(b)] or counterclockwise.⁶⁻⁸ The corresponding twins lead to eight, instead of four, Bragg spots for the magnetic $\{1,0,1\}$ peaks projecting on the $(H, K, 0)$ plane. As energy transfer is increased, these spots broaden [Figs. 2(a) and 2(b)] and then develop into well-resolved circular rings above ~ 30 meV [Figs. 2(c)–2(g)]. The spin-wave dispersions along the high symmetry direction $[100]$ and $[110]$ are demonstrated in Figs. 3(a) and 3(b), respectively. There exists featureless scattering below 40 meV whose intensity increases with Q , so it is attributed to multiphonon scattering.

Across an energy gap, and above the acoustic branch, are two optic branches. Another gap proceeds a third optic branch at higher energy. The projection of the optical modes at 110 ± 3 meV and 205 ± 15 meV on the $(H, K, 0)$ plane are shown in Figs. 4(a) and 4(c), respectively. To obtain eigenvalues of the optic modes at high symmetry points, constant- Q cuts at peak and background positions were performed and their difference was fit to a Lorentzian. Example curves and fits are shown in Figs. 4(b) and 4(d). The peak at $E = 209(1)$ meV in Fig. 4(d) presents the highest energy magnetic excitation mode in $(\text{Tl,Rb})_2\text{Fe}_4\text{Se}_5$.

At the low-energy end, the single-ion anisotropy Δ in Eq. (1) breaks the Heisenberg spin rotation symmetry, thus opening a gap in acoustic spin waves at magnetic Bragg points. The interplane coupling J_c , which stabilizes the antiferromagnetic order at finite temperature, also introduces a modulation in spin-wave dispersion along the c axis.

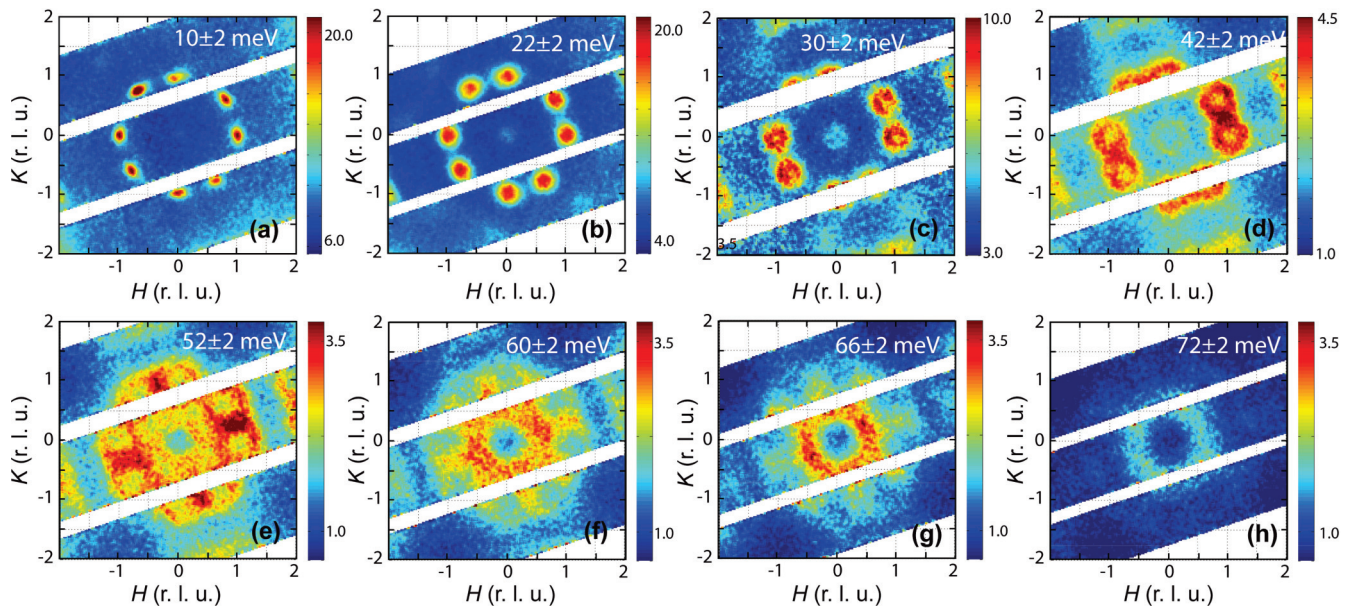


FIG. 2. (Color online) Constant energy slices of the acoustic branch of the spin-wave excitations projected on the $(H, K, 0)$ plane. The energy transfer is specified on each figure. The relative intensity is indicated by the color scale. The sample was aligned on one of the two crystalline twins in the $14/m$ unit cell. The data were collected at SEQUOIA with $E_i = 50$ meV for (a),(b) and 100 meV for the other panels.

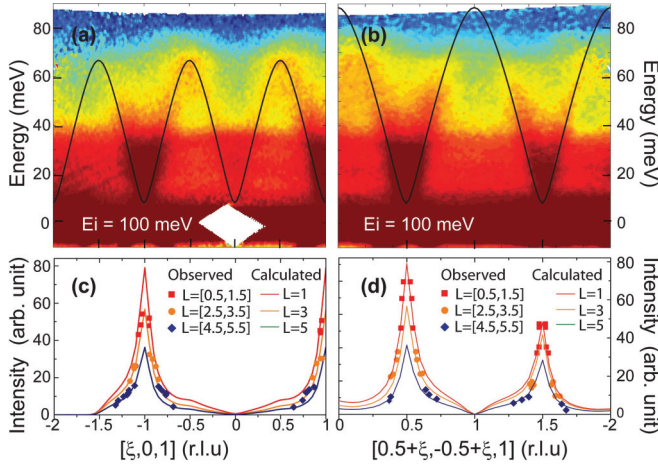


FIG. 3. (Color online) Slices of the spin-wave spectrum (a) along the [100] and (b) the [110] direction, measured with $E_i = 100$ meV. The solid line is the theoretical spin-wave dispersion described in the text. The spectral weight of the acoustic branch along the (c) [100] and (d) [110] direction was obtained from the constant- E cuts at different L values. The solid lines are calculated intensities at corresponding L .

Figures 5(a) and 5(b) show the details of the low-energy spin-wave excitations obtained with the finer E -resolution spectrometer configuration of $E_i = 50$ meV. The energy gap in magnetic excitations is obvious. Constant- Q cut through the magnetic zone center (background) is shown in Fig. 5(c). The difference intensity was fit to a step function convoluted with the instrumental resolution to obtain the intrinsic gap value 6.5(3) meV. In Fig. 5(b), the dispersive curve of bandwidth ~ 18 meV along the c axis is clearly observed.

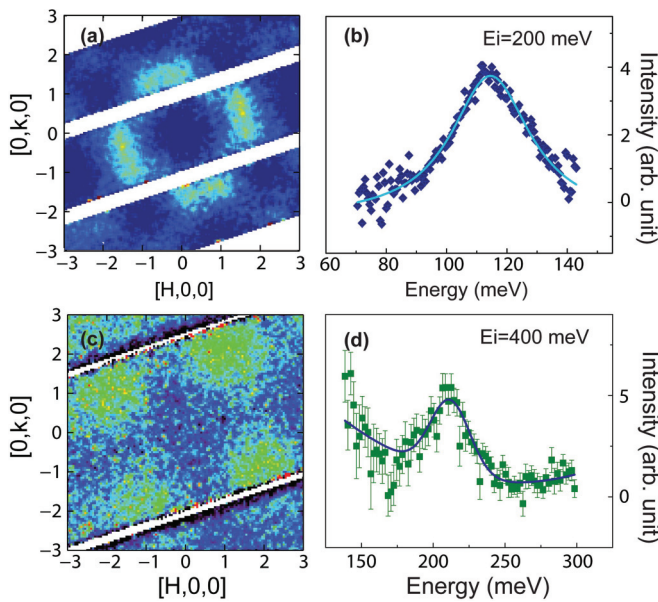


FIG. 4. (Color online) Constant energy slices of the optic branches of the spin-wave excitations projected on the $(H,K,0)$ plane at the energy transfer of (a) $E = 107$ – 113 meV and (c) $E = 190$ – 220 meV. (b) The constant- Q cut at $(1.5, 0.5, 0)$ with a background at $(3, -1, 0)$ subtracted. (d) The constant- Q cut at $(2, 1, 0)$ with a background at $(3, 1, 0)$ subtracted.

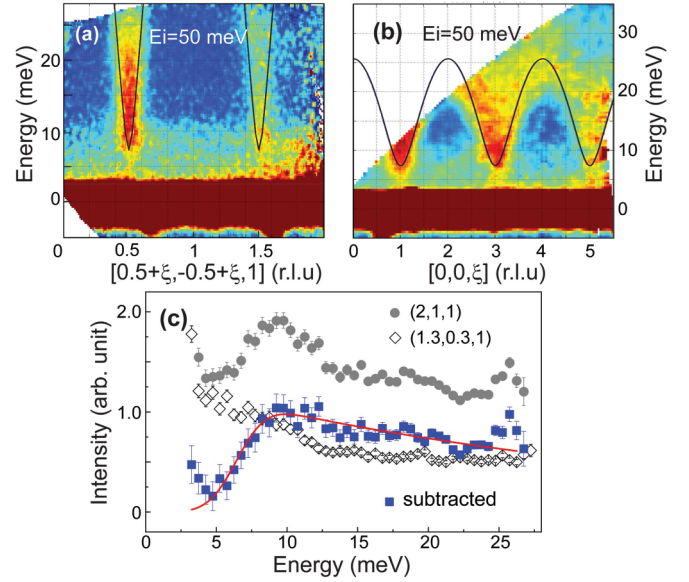


FIG. 5. (Color online) Slices of the acoustic spin-wave branch along (a) the [110] and (b) the [001] direction. (c) Constant- Q cuts through the magnetic Bragg point $(2,1,1)$ and the background point $(1.3,0.3,1)$. The difference intensity curve was fitted to the spin-wave excitations convoluted with the instrumental resolution to obtain the energy gap at 6.5(3) meV.

The simultaneous fit of the data from all branches along the multiple symmetry directions measured in this experiment to the spin-wave solution of Eq. (1) yields the following parameters:

$$\begin{aligned} SJ_1 &= -30(1) \text{ meV}, & SJ'_1 &= 31(13) \text{ meV}, \\ SJ_2 &= 10(2) \text{ meV}, & SJ'_2 &= 29(6) \text{ meV}, \\ SJ_c &= 0.8(1) \text{ meV}, & S\Delta &= 0.3(1) \text{ meV}. \end{aligned} \quad (2)$$

The resulting spin-wave dispersion curves in various high symmetry directions are shown in Fig. 1(c). They are also reproduced as the solid lines in Figs. 3(a), 3(b), 5(a), and 5(b), and are in excellent agreement with the measurements. To further check the reliability of the fits, the inelastic neutron scattering intensity was also calculated using these fitting parameters and overplotted with the observed intensity in Figs. 3(c) and 3(d). The theory agrees well with experimental results.

The J_1 , J'_1 , J'_2 , J_c and Δ in Eqs. (2) have the correct sign to stabilize the observed block antiferromagnetic order, while the weaker antiferromagnetic J_2 frustrates the ferromagnetically aligned spin block [Fig. 1(b)]. The strong difference of the exchange constants between the intra- and interblock nearest neighbor and next nearest neighbor Fe spin pairs highlights the electronic consequence of the lattice tetramerization in the $\sqrt{5} \times \sqrt{5}$ structure uncovered in structural refinement studies^{6,8} and emphasized by electronic structure calculations.^{24,27,28} In particular, the recent *ab initio* linear response theory concludes that the significant in-plane exchange interactions include only J_1 , J_2 , J'_1 , and J'_2 , whose calculated values,²⁷ remarkably, agree with our experimental results in Eqs. (2) qualitatively.

The block antiferromagnetic order not only exists in superconducting samples, but also in insulating samples with a less ordered $\sqrt{5} \times \sqrt{5}$ vacancy structure. Experimentally, this type of order is observed even for 29% filling of the vacant Fe site¹⁰ and *ab initio* calculations at 25% filling support the stability of the block antiferromagnetic order.²⁷ Recently, the spin dynamics in an insulating $\text{Rb}_{0.89}\text{Fe}_{1.58}\text{Se}_2$ sample with the block antiferromagnetic order were investigated with inelastic neutron scattering.²⁹ The overall energy scale of spin dynamics is similar to the system under study in this paper. However, the published analysis of that data provides a somewhat anomalous result as compared to our result and the aforementioned *ab initio* works. Specifically, their data could be least-squared fit only by a model that includes an interblock J_3 term in Eq. (1), where the preponderance of other results finds no need for this term. This discrepancy can be reconciled in two ways. One is to introduce a subtle physical effect in the *ab initio* studies that makes the insulating sample subtly different from the superconducting sample. The other is to consider a small overlap of the observed excitation with the \mathbf{Q} -resolution tail of its twin. We minimized this latter effect in our data by using the fine \mathbf{Q} resolution of SEQUOIA for our acoustic mode measurements.

In addition to the observed block antiferromagnetic order,^{6,7,10} many other magnetic order configurations are possible with the Heisenberg model Eq. (1) with in-plane exchange interaction extending only to the next nearest neighbors on the $\sqrt{5} \times \sqrt{5}$ vacancy ordered lattice. Theoretical work has investigated the stability of these spin configurations.^{24–26} According to the calculated phase diagram,²⁶ the exchange constants determined in the present study put $(\text{Tl,Rb})_2\text{Fe}_4\text{Se}_5$ near the boundary between the block antiferromagnetic phase and a noncollinear antiferromagnetic phase. Furthermore, such a noncollinear antiferromagnetic order has recently been observed in a spin-flop transition from the block antiferromagnetic order at 100 K in $\text{TlFe}_{1.6}\text{Se}_2$ (or $\text{Tl}_{2.5}\text{Fe}_4\text{Se}_5$).³⁰ Therefore, we postulate that composition tuning has pushed $\text{Tl}_{2.5}\text{Fe}_4\text{Se}_5$ just across this phase boundary.

The success of the Heisenberg localized spin model in describing spin dynamics in the $(\text{Tl,Rb})_2\text{Fe}_4\text{Se}_5$ superconductor may be attributed to the fact that the observed saturated magnetic moment $3.2(1)\mu_B/\text{Fe}$ is very large.⁷ Therefore, the system is close to the local spin limit. In the iron chalcogenide $\text{Fe}_{1+y}\text{Te}_{1-x}\text{Se}_x$ superconductors without the intercalating layer and Fe vacancies, the spin excitations belong to the itinerant class as those in the antiferromagnet Cr

which are described by more complex theories than linearized spin-wave theory.^{31,32} Even so, the binary iron chalcogenides are not simple antiferromagnetic metal like Cr. Their parent compounds have a magnetic wave vector that cannot be accounted for by Fermi surface nesting, and have the largest saturated magnetic moment ($2\mu_B/\text{Fe}$) among the previously discovered families of Fe-based superconductors.³³

Moreover, an additional diffusive spin excitation component in the binary iron chalcogenides was recently resolved as originating from interstitial Fe-induced short-range spin plaquettes that contain the same four-spin blocks as found in the block antiferromagnetic order.³⁴ Such fluctuating spin quartets have been shown to contribute pronounced features in the spin dynamics in the parent compound $\text{FeTe}_{1.1}$.³⁵ The close link among these antiferromagnetic states discovered experimentally in iron chalcogenides with or without vacancies was anticipated in a manganite-like theory including both itinerant and localized electronic states.²⁸

In summary, in this inelastic neutron scattering work, we contribute fresh insights to the understanding of iron chalcogenide superconductors by determining the spin Hamiltonian for a block antiferromagnetic order in the $(\text{Tl,Rb})_2\text{Fe}_4\text{Se}_5$ superconductor. Our results agree with the majority of theoretical studies that state that the dominant exchange interactions extend only to the next nearest neighbor Fe pairs in the plane. The block antiferromagnetic order is frustrated only by the intrablock next nearest exchange J_2 , the weakest among the four dominant in-plane exchange interactions. Combining our experimental exchange parameters with theoretical calculations shows that this system is near the boundary of the block antiferromagnetism regime. A unified theoretical framework for all observed types of magnetic order in the Fe-based superconductors should progress based on the experimental findings presented here.

We thank A. I. Kolesnikov, C. Cao, J. Dai, W. Ku, and D.-H. Lee for fruitful discussions. The works at RUC and ZU were supported by the National Basic Research Program of China Grants No. 2012CB921700, No. 2011CBA00112, No. 2011CBA00103, No. 2012CB821404, and No. 2009CB929104 and by the National Science Foundation of China Grants No. 11034012, No. 11190024, No. 10974175, and No. 11204059. This research at the Oak Ridge National Laboratory was sponsored by the Scientific User Facilities Division, Materials Sciences and Engineering Division, and Office of Basic Energy Sciences, US Department of Energy.

*wbao@ruc.edu.cn

¹J. Guo, S. Jin, G. Wang, S. Wang, K. Zhu, T. Zhou, M. He, and X. Chen, *Phys. Rev. B* **82**, 180520(R) (2010).

²A. Krzton-Maziopa, Z. Shermadini, E. Pomjakushina, V. Pomjakushin, M. Bendele, A. Amato, R. Khasanov, H. Luetkens, and K. Conder, *J. Phys.: Condens. Matter* **23**, 052203 (2011).

³M.-H. Fang, H.-D. Wang, C.-H. Dong, Z.-J. Li, C.-M. Feng, J. Chen, and H. Q. Yuan, *Europhys. Lett.* **94**, 27009 (2011).

⁴A. F. Wang, J. J. Ying, Y. J. Yan, R. H. Liu, X. G. Luo, Z. Y. Li, X. F. Wang, M. Zhang, G. J. Ye, P. Cheng, Z. J. Xiang, and X. H. Chen, *Phys. Rev. B* **83**, 060512 (2011).

⁵H.-D. Wang, C.-H. Dong, Z.-J. Li, Q.-H. Mao, S.-S. Zhu, C.-M. Feng, H. Q. Yuan, and M.-H. Fang, *Europhys. Lett.* **93**, 47004 (2011).

⁶W. Bao, Q.-Z. Huang, G.-F. Chen, M. A. Green, D.-M. Wang, J.-B. He, and Y.-M. Qiu, *Chin. Phys. Lett.* **28**, 086104 (2011).

⁷F. Ye, S. Chi, W. Bao, X. F. Wang, J. J. Ying, X. H. Chen, H. D. Wang, C. H. Dong, and M. Fang, *Phys. Rev. Lett.* **107**, 137003 (2011).

⁸P. Zavalij, W. Bao, X. F. Wang, J. J. Ying, X. H. Chen, D. M. Wang, J. B. He, X. Q. Wang, G. F. Chen, P.-Y. Hsieh, Q. Huang, and M. A. Green, *Phys. Rev. B* **83**, 132509 (2011).

- ⁹J. Bacsá, A. Y. Ganin, Y. Takabayashi, K. E. Christensen, K. Prassides, M. J. Rosseinsky, and J. B. Claridge, *Chem. Sci.* **2**, 1054 (2011).
- ¹⁰W. Bao, G.-N. Li, Q.-Z. Huang, G.-F. Chen, J.-B. He, D.-M. Wang, M. A. Green, Y.-M. Qiu, J.-L. Luo, and M.-M. Wu, *Chin. Phys. Lett.* **30**, 027402 (2013).
- ¹¹Z. Wang, Y. J. Song, H. L. Shi, Z. W. Wang, Z. Chen, H. F. Tian, G. F. Chen, J. G. Guo, H. X. Yang, and J. Q. Li, *Phys. Rev. B* **83**, 140505 (2011).
- ¹²D. H. Ryan, W. N. Rowan-Weetaluktuk, J. M. Cadogan, R. Hu, W. E. Straszheim, S. L. Budko, and P. C. Canfield, *Phys. Rev. B* **83**, 104526 (2011).
- ¹³A. Ricci, N. Poccia, G. Campi, B. Joseph, G. Arrighetti, L. Barba, M. Reynolds, M. Burghammer, H. Takeya, Y. Mizuguchi, Y. Takano, M. Colapietro, N. L. Saini, and A. Bianconi, *Phys. Rev. B* **84**, 060511(R) (2011).
- ¹⁴Z. Shermadini, A. Krzton-Maziopa, M. Bendele, R. Khasanov, H. Luetkens, K. Conder, E. Pomjakushina, S. Weyeneth, V. Pomjakushin, O. Bossen, and A. Amato, *Phys. Rev. Lett.* **106**, 117602 (2011).
- ¹⁵A. M. Zhang, J. H. Xiao, Y. S. Li, J. B. He, D. M. Wang, G. F. Chen, B. Normand, Q. M. Zhang, and T. Xiang, *Phys. Rev. B* **85**, 214508 (2012).
- ¹⁶P. J. Hirschfeld, M. M. Korshunov, and I. I. Mazin, *Rep. Prog. Phys.* **74**, 124508 (2011).
- ¹⁷Y.-Z. You, F. Yang, S.-P. Kou, and Z.-Y. Weng, *Phys. Rev. Lett.* **107**, 167001 (2011).
- ¹⁸M. Khodas and A. V. Chubukov, *Phys. Rev. Lett.* **108**, 247003 (2012).
- ¹⁹M. Stone, M. Loguillo, and D. Abernathy, *Rev. Sci. Instrum.* **82**, 055117 (2011).
- ²⁰G. E. Granroth, D. H. Vandergriff, and S. E. Nagler, *Physica B* **385-386**, 1104 (2006).
- ²¹G. E. Granroth, A. I. Kolesnikov, T. E. Sherline, J. P. Clancy, K. A. Ross, J. P. C. Ruff, B. D. Gaulin, and S. E. Nagler, *J. Phys.: Conf. Ser.* **251**, 012058 (2010).
- ²²D. L. Abernathy, M. B. Stone, M. J. Loguillo, M. S. Lucas, O. Delaire, X. Tang, J. Y. Y. Lin, and B. Fultz, *Rev. Sci. Instrum.* **83**, 015114 (2012).
- ²³T. Yildirim, *Phys. Rev. Lett.* **101**, 057010 (2008).
- ²⁴C. Cao and J. Dai, *Phys. Rev. Lett.* **107**, 056401 (2011).
- ²⁵Y.-Z. You, H. Yao, and D.-H. Lee, *Phys. Rev. B* **84**, 020406(R) (2011).
- ²⁶R. Yu, P. Goswami, and Q. Si, *Phys. Rev. B* **84**, 094451 (2011).
- ²⁷L. Ke, M. van Schilfgaarde, and V. Antropov, *Phys. Rev. B* **86**, 020402(R) (2012).
- ²⁸W.-G. Yin, C.-H. Lin, and W. Ku, *Phys. Rev. B* **86**, 081106(R) (2012).
- ²⁹M. Wang, C. Fang, D.-X. Yao, G. Tan, L. W. Harriger, Y. Song, T. Netherton, C. Zhang, M. Wang, M. B. Stone, W. Tian, J. Hu, and P. Dai, *Nat. Commun.* **2**, 580 (2011).
- ³⁰A. F. May, M. A. McGuire, H. Cao, I. Sergueev, C. Cantoni, B. C. Chakoumakos, D. S. Parker, and B. C. Sales, *Phys. Rev. Lett.* **109**, 077003 (2012).
- ³¹M. D. Lumsden, A. D. Christianson, E. A. Goremychkin, S. E. Nagler, H. A. Mook, M. B. Stone, D. L. Abernathy, T. Guidi, G. J. MacDougall, C. de la Cruz, A. S. Sefat, M. A. McGuire, B. C. Sales, and D. Mandrus, *Nature Phys.* **6**, 182 (2010).
- ³²D. N. Argyriou, A. Hiess, A. Akbari, I. Eremin, M. M. Korshunov, J. Hu, B. Qian, Z. Mao, Y. Qiu, C. Broholm, and W. Bao, *Phys. Rev. B* **81**, 220503(R) (2010).
- ³³W. Bao, Y. Qiu, Q. Huang, M. A. Green, P. Zajdel, M. R. Fitzsimmons, M. Zhernenkov, S. Chang, M. Fang, B. Qian, E. K. Vehstedt, J. Yang, H. M. Pham, L. Spinu, and Z. Q. Mao, *Phys. Rev. Lett.* **102**, 247001 (2009).
- ³⁴V. Thampy, J. Kang, J. A. Rodriguez-Rivera, W. Bao, A. T. Savici, J. Hu, T. J. Liu, B. Qian, D. Fobes, Z. Q. Mao, C. B. Fu, W. C. Chen, Q. Ye, R. W. Erwin, T. R. Gentile, Z. Tesanovic, and C. Broholm, *Phys. Rev. Lett.* **108**, 107002 (2012).
- ³⁵I. A. Zaliznyak, Z. Xu, J. M. Tranquada, G. Gu, A. M. Tsvelik, and M. B. Stone, *Phys. Rev. Lett.* **107**, 216403 (2011).